1-2021

High-temperature Performance of Ambient-cured Alkali- Activated Binder Concrete

Kruthi Kiran Ramagiri
BITS-Pilani Hyderabad Campus

Darshan Chauhan
Portland State University, drc9@pdx.edu

Shashank Gupta
Politecnico di Milano

Arkamitra Kar
Birla Institute of Technology and Science (BITS)

Dibyendu Adak
NIT Meghalaya

See next page for additional authors

Citation Details

Published as: Ramagiri, K.K., Chauhan, D.R., Gupta, S. et al. High-temperature performance of ambient-cured alkali-activated binder concrete. Innov. Infrastruct. Solut. 6, 71 (2021). https://doi.org/10.1007/s41062-020-00448-y

High-temperature Performance of Ambient-cured Alkali-Activated Binder Concrete

Kruthi Kiran Ramagiri[1]

PhD Candidate, Department of Civil Engineering, BITS-Pilani Hyderabad Campus, Hyderabad, India.

E-mail: p20170008@hyderabad.bits-pilani.ac.in

ORCID iD: 0000-0001-8801-6581

Darshan Rajesh Chauhan

Graduate Student, Department of Civil and Environmental Engineering, Portland State University, OR, USA.

E-mail: drc1807@gmail.com

Shashank Gupta

Graduate Student, Civil, Environmental and Land Management Engineering, Politecnico di Milano, Milan, Italy.

E-mail: shashankgupta196@gmail.com

Arkamitra Kar

Assistant Professor, Department of Civil Engineering, BITS-Pilani Hyderabad Campus, Hyderabad, India.

E-mail: arkamitra.kar@hyderabad.bits-pilani.ac.in

ORCID iD: 0000-0002-7215-7491

Dibyendu Adak

Assistant Professor, Civil Engineering, NIT Meghalaya, Shillong, India.

E-mail: dibu.ce@gmail.com

Abhijit Mukherjee

Professor, Faculty of Science and Engineering, School of Civil and Mechanical Engineering, Bentley Campus, Curtin University, Bentley, Australia.

E-mail: Abhijit.Mukherjee@curtin.edu.au

[1]Corresponding author

High-temperature Performance of Ambient-cured Alkali-Activated Binder Concrete

Abstract

Owing to their lower carbon footprint and efficient performance compared to portland cement (PC), alkali-activated binders (AAB) show promising potential as an alternative to PC. The present paper investigates the high-temperature performance of AAB concrete through compressive and bond strength tests. Four different AAB concrete mixes with varying proportions of fly ash: slag (100:0, 70:30, 60:40, and 50:50) cured under ambient conditions are exposed to elevated temperatures. The mechanical performance of AAB concrete is corroborated with microstructural changes. The results show that AAB concrete with fly ash: slag ratio of 70:30 exhibits the best mechanical performance after exposure to elevated temperatures. This behaviour is attributed to the growth of new crystalline phases of akermanite and gehlenite as observed from the X-ray diffraction patterns. This study shows that there is an optimum proportion of slag content beyond which the mechanical performance of AAB concrete significantly deteriorates when exposed to elevated temperatures. The failure pattern of AAB concrete during the bond strength test varies with the precursor proportion and the exposure condition.

Keywords: Alkali-activated binders; ambient-curing; bond strength; elevated temperature; microstructure.

Declarations

Funding: This study is sponsored by BITS Pilani, Hyderabad campus through Outstanding Potential for Excellence in Research and Academics (OPERA) grant.

Conflicts of interest/Competing interests: There are no conflicts of interest.

Availability of data and material: All the required data are available in the manuscript, and all the raw data are available upon request in MS-Excel format.

Code availability: Not Applicable

1. Introduction

Augmented need for sustainable alternatives to portland cement (PC) resulted in increasing investigations on the potential replacements like alkali-activated binders (AAB). Traditionally, AAB concrete has been produced through thermal curing at temperatures in the range of 60 °C to as high as 150 °C. In a drive towards reducing this extensive consumption of energy and promoting widespread application, the focus of this study is to investigate the characteristics of AAB concrete cured at ambient conditions. It is now quite commonly known that AAB is produced by the alkaline activation of aluminosilicate-rich precursors such as fly ash and/or slag. Upon hardening, concrete made with this binder exhibits properties similar or even superior to its PC counterpart. AAB concrete exhibits enhanced mechanical strength [1], higher resistance to acid attack [2], chloride ingress [3], and alkali-silica reaction [4].

The durability of concrete is critical, especially when exposed to extreme conditions such as seawater, fire accidents, and alternate freezing and thawing. Increasing infrastructure around the world with more fire risk structures such as concrete tunnels, nuclear reactors, and oil refineries led to escalated demand for highly fire-resistant concrete [5]. Research thus far suggests that, unlike PC, thermally-cured AAB concrete exhibits adequate fire endurance in terms of both spalling resistance and residual strength at elevated temperatures [5]. PC concrete is incombustible, good insulating material and has low thermal diffusivity compared to timber or steel [6]. However, conventional PC concrete suffers deterioration of its mechanical properties and explosive spalling on exposure to high temperatures. On exposure to temperatures in the range of 400-600 °C, PC concrete exhibits a decline in its strength due to decomposition of portlandite ($Ca(OH)_2$) [7] and C-S-H phases [8] accompanied by loss of chemically bound water. AAB concrete is found to retain a significant proportion of its residual strength under similar exposure conditions [8]. With an increase in temperatures beyond 600 °C, the entire structural integrity of PC concrete is compromised. However, AAB concrete exhibits a pseudo-viscous phase, owing to the sintering of precursors, elucidating its improved mechanical performance when exposed to severely high temperatures [9].

The responses of AAB and PC concrete on exposure to elevated temperatures are vastly different. The type of precursors used and the distinct chemistry of the reaction products are determinants for the distinct behaviour of AAB and PC concrete. The precursors and the reaction products subsequently govern the porosity and hence the resistance of hardened concrete to elevated temperatures. Existing research on AAB indicates that its residual strength depends on its initial strength. With an increase in initial strength, the residual strength decreases exponentially. Specimens with low initial strength exhibit improvement up to 90 % on exposure to 800 °C. This behaviour is attributed to further polymerization of the unreacted particles. Specimens with high strength exhibited strength loss up to 70-90 % [10, 11]. The residual strength of AAB can increase or decrease on exposure to high-temperature contingent to thermal incompatibility, pore pressure and phase transformations [11].

The enhanced spalling resistance of AAB concrete, specifically with fly ash as a precursor is attributed to its open pore structure in contrast to metakaolin based AAB or PC concrete [12, 13]. Studies using fly ash from different sources conclude that the performance of fly ash-based AAB degrades with increasing iron content in fly ash [14]. The formation of new phases and sintering of the matrix is observed in fly ash and blended AAB. Unlike fly ash-based AAB, the residual strength of alkali-activated slag concrete decreases after exposure to high temperature. The dominating effect in alkali-activated slag is the formation of macrocracks due to the temperature gradient and pore pressure [15]. A contradictory study to the findings discussed above reported an increase in strength, as high as 47 %, in AAB with slag and PC as binders after exposure to 800 °C [16]. Some studies have reported variations in the performance of

AAB concrete exposed to elevated temperatures with size and type of the aggregate, size of the specimen, curing temperature, and the type of activators used [17, 18]. However, most studies [7, 14, 17, 18] adopted heat-curing of the specimens, which is feasible in precast concrete production plants but limits in-situ applications of AAB concrete. So, there is a need to determine the response to elevated temperatures for AAB concrete cured under ambient conditions.

When reinforced concrete is to be used in a fire-resistant structure, the critical parameter governing its mechanical behaviour at elevated temperatures is the bond between embedded steel and concrete. This bond between embedded steel and concrete predominantly governs the effective performance of reinforced concrete as a composite material. The load transfer between concrete and steel usually referred to as bond, is idealized as a constant stress field developed at the steel-concrete interface. Hence, it is crucial to examine this bond behaviour of AAB concrete for it to be used as a replacement for PC concrete. Studies investigating the effect of mix proportions, curing conditions, the source of precursors, concrete cover, diameter and type of rebar, bond length on the bond strength of AAB concrete are reported in the literature [19-23]. Some studies conducted on AAB concrete using pull-out test reported its superior bond behaviour compared to PC concrete [20, 24]. This behaviour is attributed to greater tensile strength and the compact interfacial transition zone (ITZ) of AAB concrete [20, 24]. When smaller diameter rebars are used, a strong bond between rebar and concrete always resulted in the failure due to the breaking of the bar rather than slippage [24]. In contrast, specimens with larger size bars experienced failure due to the splitting of concrete. Curing conditions govern the bond behaviour of class F fly ash based AAB concrete. The bond strength of AAB concrete improved with the duration of heat curing [21]. The nano-silica modified geopolymer concrete displayed superior bond performance in contrast to PC concrete, with both mild and deformed steel bars [19]. More recently, the effect of type and content of fly ash, sodium silicate/sodium hydroxide (Na_2SiO_3/NaOH) ratio and water content on the bond strength of fly ash-based AAB concrete have been examined [25]. All of the studies mentioned above examined the bond strength of reinforced AAB concrete cured at elevated temperatures varying in the range of 35-80 °C for 24 - 48 hours [19- 22, 24, 25]. Relevant information is not reported in the case of ambient-cured AAB concrete.

Additionally, only limited research is available on bond behaviour of AAB concrete on exposure to elevated temperatures. A recent study reported that the degradation rate of the bond strength of metakaolin and fly ash-blended AAB concrete exposed to elevated temperatures is similar to that of its splitting tensile strength. This rate of decrease in bond strength is higher compared to that of the compressive strength of AAB concrete [26]. However, there is no reported study on the bond strength for concrete prepared with (fly ash + slag)-based AAB under ambient curing conditions.

Based on these findings, this study is aimed at achieving the following objectives: i) to investigate the compressive and bond strength of ambient-cured AAB concrete when exposed to elevated temperatures and ii) to evaluate the effect of varying proportions of fly ash and slag on the compressive and bond strength of AAB concrete under ambient curing conditions and determine an optimum precursor combination. The observations are then correlated with microstructural changes determined for hardened AAB paste samples from existing literature, as detailed later in the manuscript [27]. The broad goal of this study is to help in promoting the in-situ use of ambient-cured AAB concrete in engineering applications where the primary purpose is to resist elevated temperatures or fire attacks. The materials and detailed experimental methodology used for this study are presented in the following section.

2. Materials and methods

2.1. Materials

Class F fly ash with a specific gravity of 2.04 was procured from National Thermal Power Corporation (NTPC) Ramagundam, from the state of Telangana, India and complied with the specifications of ASTM C618 [28]. Ground granulated blast furnace slag (slag) with a specific gravity of 2.71 used in this study was obtained from JSW Cement Ltd and conformed to the specifications of ASTM C989 / C989M [29]. Table 1 presents the oxide composition of fly ash and slag used in this study.

Table 1 Properties of precursors

Components (%)	Fly ash	Slag
CaO	1.78	40.64
SiO_2	60.13	35.15
Al_2O_3	28.37	19.60
Fe_2O_3	5.10	0.53
SO_3	0.11	1.89
K_2O	2.16	0.40
TiO_2	1.42	0.92
Specific surface area (m^2/kg)	490	580

For preparation of the alkali-activator solution, sodium hydroxide flakes (NaOH) and sodium silicate (Na_2SiO_3) solution were used. Rayon grade NaOH flakes with 99 % purity and industrial-grade Na_2SiO_3 solution with 29.5 % SiO_2 and 14.7 % Na_2O by weight supplied by HYCHEM laboratories are utilized. In order to allow sufficient time for dissipation of heat, the activating solution was prepared a day before the usage.

Natural siliceous sand sieved through 4.75 mm conforming to Zone II as per IS 383 – 2016 was used as fine aggregate [30]. Crushed granite aggregate of 10 mm nominal maximum size was used as coarse aggregate. The physical properties of the aggregates are presented in Table 2. Polycarboxylic ether-based high-range water-reducing admixture procured from BASF chemicals was used as superplasticizer (SP). For the bond strength of concrete, deformed steel bars (0.2 % proof stress = 500 MPa) of 12 mm diameter were used in the present study.

Table 2. Physical properties of aggregates

Aggregate	Specific gravity	Water absorption (%)
Coarse aggregate	2.72	0.1
Fine aggregate	2.65	0.5

2.2.Mix proportions and specimen preparation

In this study, four different mixes with varying proportions of fly ash and slag ratios were selected for the preparation of AAB specimens. Fly ash: slag ratios of 100:0 (FS 0), 70:30 (FS 30), 60:40 (FS 40), and 50:50 (FS 50) were used in the present study. A blend containing a mixture of NaOH and Na_2SiO_3 is used as the activator for preparing the alkaline solution. From

the findings of a previous study, the suggested Ms modulus (SiO_2/Na_2O ratio in the activating solution) of 1.4 was used in the present study [31]. The water-to-solids (w/s) ratio for AAB concrete was maintained at 0.3, to achieve desired workability without adding SP for FS 0. This w/s ratio ensured the addition of a limited quantity of SP for the other AAB concrete mixes. For calculating the w/s ratio, water content is considered to be the sum of additional water, and the water present in Na_2SiO_3 solution whereas the solids include binders, NaOH and the solids in Na_2SiO_3 solution. The mix details are presented in Table 3.

Table 3 Mix details of AAB concrete

Materials	FS 0	FS 30	FS 40	FS 50
Fly ash (kg/m^3)	400	280	240	200
Slag (kg/m^3)	0	120	160	200
Sodium Hydroxide Pellets (kg/m^3)	10.57	10.57	10.57	10.57
Sodium Silicate Solution (kg/m^3)	129.43	129.43	129.43	129.43
Coarse Aggregate (kg/m^3)	1209	1209	1209	1209
Fine Aggregate (kg/m^3)	651	651	651	651
Additional water (kg/m^3)	77.38	77.38	77.38	77.38
SP (l/m^3)	0	3.14	3.57	4

The preparation of AAB concrete specimens commenced with the blending of dry ingredients viz. coarse aggregates, fine aggregates followed by fly ash and slag. Then the activating solution was added to the mix. A measured quantity of water (in addition to water content in Na_2SiO_3 solution) followed by SP, if required, was then added to obtain a uniform blend. The age of demoulding the specimens varied depending on the content of fly ash in the mix owing to its slow reactivity. All the specimens were demoulded after gaining sufficient strength to impede any damage. FS 0 specimens were demoulded at the age of 7 days. FS 30, FS 40, and FS 50 specimens were demoulded at the age of 2 days. On demoulding, the specimens were cured until 7-day age underwater and then under ambient laboratory conditions until the commencement of tests. The average ambient temperature was 25 °C, and the relative humidity was in the range of 60-75 % in Hyderabad. This curing regime is selected based on the recommendations of previous research on blended AAB [32, 33]. The existing research indicates that underwater curing of AAB is beneficial at early ages (1-7 days) rather than at 28 days. Intermittent water curing (7 days underwater and 21 days of air curing) is reported to be efficient in developing satisfactory 28-day compressive strength [32, 33]. Furthermore, complying with the broad goal of this study to promote in-situ applications, ambient curing is adopted. The relevant experimental methodology is presented in the following section. In the present study, all the samples are tested at the age of 28 days.

2.3.Experimental Methods

This study determines the influence of exposure to severely high temperatures on the compressive and bond strength values of ambient-cured AAB concrete. The correlation between the mechanical performance and the microstructural changes are also analyzed. The microstructural analyses for the paste samples considered in the present paper for the selected

exposure conditions were performed and presented in detail as part of a previous study by the current authors [27]. In the present study, the mechanical performance of ambient-cured AAB concrete before and after exposure to high temperatures is corroborated with the microstructural changes.

2.3.1. Mineralogical and microstructural analysis

The parameters used for X-ray diffraction (XRD) analysis comprise CuKα X-rays operated at 40 kV and 30 mA with a scan speed of 1 °/min, a step width of 0.02 ° and a 2θ range of 5 to 90 °. Fourier Transform Infrared Spectroscopy (FTIR) analysis was performed with a resolution of 4 $cm^{-1,}$ and KBr pellet technique was used for sample preparation. Scanning electron microscopy coupled with energy-dispersive X-ray spectroscopy (SEM-EDS) analysis was performed for an oven-dried sample sputtered with a gold-palladium layer of 10 nm thickness. The sample for SEM-EDS analysis was prepared using a method specified in a previous study on AAB [34].

2.3.2. Exposure to elevated temperature

The specimens were exposed to elevated temperatures selected based on the standard time-temperature curve specified by ASTM E119 [35]. Four different exposure conditions – ambient temperature, 538 °C, 760 °C, and 892 °C were selected to study the performance of matured AAB concrete upon exposure to elevated temperatures. On the day of testing, the specimens were exposed to elevated temperatures in a muffle furnace supplied by Aimil Ltd for 2 hours. Existing literature on AAB reported that a state of thermal equilibrium was reached when the specimens were preserved at the exposed temperature for 2 hours [36, 37]. The furnace temperature was increased from room temperature to the designated elevated temperature to comply with the standard time-temperature curve as specified by ASTM E119. After 2-hour exposure to elevated temperature, the specimens are gradually allowed to cool down to the room temperature.

For each exposure condition, compressive and bond strength tests are replicated for four different mixes viz. FS 0, FS 30, FS 40, and FS 50.

2.3.3. Compressive Strength

Compressive strength test was performed on cylindrical concrete specimens of 150 mm diameter and 300 mm height. Specimens were cast using uniform compaction with a mechanical vibrator. The specimens were then allowed to moist-cure until the age of 7 days. After curing, the test specimens were stored at ambient temperature in the laboratory until the day of testing. All the specimens were tested at the age of 28 days. The compressive strength test of concrete was performed following specifications of ASTM C39 / C39M [38] using a compression testing machine of 2000 kN capacity.

2.3.4. Bond Strength

Bond strength of concrete was evaluated by conducting the pull-out test on the specimens with embedded rebar at the centre through an automated universal testing machine of 1000 kN capacity and a specially fabricated test frame (Figure 1). The specimens to be tested for bond behaviour were cast in a fabricated cube mould (100 × 100 × 100 mm) with a central hole to accommodate the rebar vertically. The dimensions of the cube and diameter of rebar are selected based on the specifications of the Indian standard code of practice for performing the pull-out test, IS 2770-1 [39]. Curing conditions similar to the specimens tested for compressive strength are followed. The test procedure complies with the guidelines of IS 2770-1. The test was performed in the displacement control mode with the rate of loading maintained at 0.01 mm/sec. An automated data acquisition system is used to record the load. The specimens were

subjected to loading until they reached failure. The bond strength reported is the average of three specimens. The bond strength is calculated as the ratio of applied load required for the slip to the surface area of the embedded length of the rebar. The average bond stress is calculated as:

$$\sigma_{bond} = \frac{P}{\pi dL}$$

where,

d = diameter of the reinforcement (mm)

L = length of specimen parallel to the reinforcement (mm)

P = load at specimen failure (N)

σ_{bond} = bond stress (MPa)

The results from the experiments are presented in the following section.

Insert Figure 1 here

Figure 1 Pull-out test apparatus

3. Results

3.1. Compressive strength test

The mean compressive strength values of three AAB concrete cylindrical specimens subjected to the selected exposure conditions at the age of 28 days are presented in Figure 2. It is evident from Figure 2 that the compressive strength of AAB concrete increases with slag content. The results from this study corroborate with the previous findings of the elimination of thermal curing with the inclusion of slag in AAB concrete [31]. The increase in strength with increasing slag content is attributed to the formation of the additional reaction product, calcium aluminosilicate hydrate (C-A-S-H), resulting in pore refinement [40, 41]. The increase in compactness of microstructure with slag content associated with the formation of C-A-S-H is presented in a previous study by the current authors and also other studies on blended AAB [27, 40, 41]. XRD analysis of the samples show an increase in the formation of C-A-S-H matrix with slag content (Figure 3).

Insert Figure 2 here

Figure 2 Compressive strength test results

Insert Figure 3 here

Figure 3 (a) FS 30 (b) FS 40 (c) FS 50

XRD pattern of AAB exposed to high temperature

Ac = analcime, Ak = akermanite, Al = albite, An = anorthite, C =Calcite, CS = C-A-S-H, G = gehlenite, H = Hematite, M = mullite, N = nepheline, Q = quartz, S = hydroxy sodalite

The poor mechanical performance of FS 0 under ambient exposure conditions is attributed to the absence of thermal curing. Under ambient curing conditions, the degree of hydration of fly ash is low, and hence FS 0 contains a higher proportion of unreacted fly ash particles [42]. However, with an increase in temperature to around 500 °C further geopolymerization enhances the strength [43].

The microstructure plays a significant role in governing the mechanical performance of AAB concrete, especially when exposed to high-temperature. In cementitious systems exposed to high temperatures, it is observed that the pore pressure of water developed inside the specimens

require an escape route and otherwise develop stresses on the adjacent concrete resulting in spalling, explosive or premature failure depending on its intensity [44]. This pore pressure of water is governed by the pore structure or the compactness of the microstructure. FS 50, which exhibits the highest strength at ambient exposure conditions, undergoes substantial loss in strength on exposure to 760 °C and 892 °C. This behaviour is ascertained to its dense microstructure occluding the moisture escape from the specimen. This dense microstructure of FS 50 can be substantiated by the formation of C-A-S-H.

The compressive strength of FS 30 and FS 40 also decreases with increase in temperature up to 760 °C. However, on exposure to a temperature of 892 °C, the compressive strength of both FS 30 and FS 40 increases. This behaviour is attributed to the growth of crystalline phases of akermanite ($2CaO{\cdot}MgO{\cdot}2SiO_2$) and gehlenite ($2CaO{\cdot}Al_2O_3{\cdot}SiO_2$) in AAB when exposed to temperatures higher than 760 °C [27]. Formation of akermanite and gehlenite is evident from the XRD pattern of AAB presented in Figure 3.

Insert Figure 4 here

Figure 4 FTIR spectra of AAB under ambient exposure conditions

According to available literature, slag is composed of a mixture of poorly crystalline phases with compositions resembling gehlenite and akermanite, with depolymerized calcium silicate glasses [45]. The growth of these crystals is promoted by high temperature. These crystalline phases result in the formation of a stronger bond and resulting in the transition of the binder phase. The newly formed binder at this temperature is expected to re-establish the contact with aggregates improving the mechanical performance [46]. However, the strength reduction in FS 50 validates the fact that the degradation due to pore pressure development is dominating the enhancement of strength due to the formation of crystalline phases.

The lower percentage reduction of strength in AAB concrete predominant in fly ash is due to the higher proportion of pores [27]. Fly ash is known to consist of a large number of hollow spherical particles called cenospheres at the molecular level. The authors hypothesize that when exposed to high-temperature, sintering of such fly ash particles results in a large number of highly dispersed pores. These pores provide an escape route for the moisture alleviating the damage. The increase in the number of pores in FS 0 specimens is evident from the SEM micrographs presented in Figure 5. Similar behaviour is observed in previous research on fly ash-based AAB [47].

Insert Figure 5 here

Figure 5 SEM micrographs of AAB (Magnification = 2500x)

Visual inspection of AAB concrete before and after exposure to high-temperature is presented in Figure 6a, 6b, and 6c. The colour of AAB concrete changes to auburn when exposed to 892 °C. The colour change is attributed to dehydration and oxidation of iron present in fly ash. FS 0 exhibits a light auburn colour at ambient temperature (Figure 6a).

Insert Figure 6 here

Figure 6 Comparison of the effect of high-temperature exposure on failure pattern

**AT = ambient temperature*

3.2.Bond strength test

The bond strength of AAB concrete and its behaviour on exposure to high-temperature is presented in Figure 7.

Insert Figure 7 here

Figure 7 Bond strength test results

Analogous to compressive strength results, the bond strength of AAB concrete increases with slag content under ambient exposure conditions. The bond strength of FS 50 is 122.8 % higher than FS 0. This high bond strength of FS 50 is attributed to pore refinement resulting in a relatively uniform and compact interfacial transition zone (ITZ) between the embedded rebar and concrete. The improvement in strength and interfacial binding with slag content is attributed to a relatively higher proportion of dissolved species contributing to the formation of more reaction products [48]. The pore refinement in FS 50 is validated by the formation of additional C-A-S-H matrix and a compact microstructure [27].

The bond strength of AAB concrete decreases with increasing temperature. This depletion in the bond strength is higher in AAB concrete with more slag content as the bond between the shorter C-A-S-H bonds deteriorates more than the bond between the rebars and the longer chain sodium aluminosilicate hydrate matrix (N-A-S-H) bonds. N-A-S-H is the primary reaction product of fly ash-rich AAB [45]. Since it is amorphous, it cannot be detected through XRD analysis. However, if individually considered, the microstructure of the FS 30 is denser than the FS 0. Consequently, FS 30 exhibits the highest residual bond strength at 892 °C compared to other mixes. This behaviour is attributed to the combined effect of the growth of crystalline phases (akermanite and gehlenite) densifying the matrix and the sintered fly ash particles increasing the pores allowing evaporation of moisture [27].

The specimens subjected to pull-out tests fail either due to splitting of concrete or slippage of rebar or exhibit a combination failure (Figure 6d-i). The summary of observed failures is presented in Table 4.

Table 4 Summary of observed bond failure

Mix ID	Exposure Condition	
	Ambient temperature	Elevated temperature
FS 0	Splitting of concrete	Combination failure
FS 30	Slippage of rebar	Combination failure
FS 40	Slippage of rebar	Combination failure
FS 50	Slippage of rebar	Combination failure

The factor governing the failure mode is either splitting capacity of AAB concrete or the bond capacity between the steel rebar and AAB concrete. Splitting capacity is related to the splitting tensile strength of the concrete and the concrete cover. The bond capacity depends on the geometry of rebar and compressive strength of concrete [49]. The type of failure of AAB concrete during the pull-out test is observed to be governed by the exposure conditions. At ambient exposure conditions, FS 0 exhibited splitting type of failure (Figure 6d). On exposure to high-temperatures, FS 0 revealed a combination failure due to both splitting of concrete and slippage of rebar (Figure 6e). FS 30, FS 40 and FS 50 exhibited failure due to slippage of rebar under ambient exposure conditions (Figure 6f-i). However, with an increase in temperature, these mixes also exhibited a combination failure. Therefore, it is evident that the failure of specimens exposed to high-temperature is always due to a combination of slippage of rebar and splitting of concrete. Under ambient conditions, the precursor combination governs the mode of failure. The combination failure at high-temperatures is ascertained to differential

deformations between embedded steel and AAB concrete. The coefficient of thermal expansion of concrete and steel are comparable under reference or ambient conditions. However, when exposed to elevated temperatures, differential thermal expansion of the steel rebar and the surrounding concrete was reported in previous studies on PC concrete [50, 51]. The friction between rebar and concrete, which significantly governs the bond capacity, is alleviated owing to these differential deformations. This reduction in friction also reduces the bond capacity allowing the mode of failure to transform from splitting to a combination failure.

4. Conclusion

This paper presents the high-temperature behaviour of AAB concrete exposed to a varied temperature ranging from ambient (25 °C) to 892 °C through compressive strength and pull-out tests. The findings from the present study are as follows:

- Under ambient exposure conditions, increase in slag content improved the mechanical performance of AAB concrete. This behaviour is attributed to the formation of the additional reaction product, C-A-S-H.
- On exposure to elevated temperatures, the deterioration in the mechanical performance, both compressive strength and bond strength, of AAB concrete with slag content observed in the present study is attributed to the increased compactness of the matrix.
- Fly ash: slag ratio of 70:30 is proposed as an optimum precursor combination based on the results of the present study under the locally available ambient curing and exposure conditions. AAB concrete with fly ash: slag ratio of 70:30 exhibited about 145 % higher residual compressive and 29 % higher bond strength compared to AAB concrete with fly ash: slag ratio of 50:50 when exposed 892 °C.
- The enhanced mechanical performance of AAB concrete with fly ash: slag ratio of 70:30 when exposed to a temperature higher than 760 °C is attributed to the growth of crystalline phases of akermanite and gehlenite.
- The type of failure during the pull-out test is governed by the precursor proportion and the exposure condition. The specimens failed due to a combination of splitting of concrete and slippage of rebar when exposed to high-temperature. The shift from splitting and slippage of rebar in AAB concrete with fly ash: slag ratio of 100:0 and other mixes, respectively, to a combination failure, is attributed to the differential deformations between the embedded rebar and AAB concrete.

The results from the present study provide insight into the high-temperature performance of AAB concrete and the possible associated microstructural changes. These findings on the behaviour of reinforced AAB concrete exposed to high-temperatures may be useful during practical applications of these binders.

Acknowledgements

The authors would like to acknowledge the central analytical laboratory facilities at BITS Pilani, Hyderabad campus for providing the necessary setup to conduct XRD, FTIR and SEM-EDS analyses.

References

1. Gebregziabiher BS, Thomas R, Peethamparan S (2015) Very early-age reaction kinetics and microstructural development in alkali activated slag. Cem Concr Compo 55:91-102. https://doi.org/10.1016/j.cemconcomp.2014.09.001.

2. Fernández-Jiménez A, García-Lodeiro I, Palomo A (2007) Durability of alkali-activated fly ash cementitious materials. J Mater Sci 42(9):3055-3065. https://doi.org/10.1007/s10853-006-0584-8.

3. Ravikumar D, Neithalath N (2013) Electrically induced chloride ion transport in alkali activated slag concretes and the influence of microstructure. Cem Concr Res 47:31-42. https://doi.org/10.1016/j.cemconres.2013.01.007.

4. García-Lodeiro I, Palomo A, Fernández-Jiménez A (2007) Alkali-aggregate reaction in activated fly ash systems. Cem Concr Res 37(2):175-183. https://doi.org/10.1016/j.cemconres.2006.11.002.

5. Ali AM, Sanjayan J, Guerrieri M (2017) Performance of geopolymer high strength concrete wall panels and cylinders when exposed to a hydrocarbon fire. Constr Build Mater 137:195-207. https://doi.org/10.1016/j.conbuildmat.2017.01.099

6. Khoury GA (2000) Effect of fire on concrete and concrete structures. Prog Struct Eng Mat 2(4):429-447. https://doi.org/10.1002/pse.51

7. Rashad AM, Zeedan SR (2011) The effect of activator concentration on the residual strength of alkali-activated fly ash pastes subjected to thermal load. Constr Build Mater 25(7):3098-3107. https://doi.org/10.1016/j.conbuildmat.2010.12.044

8. Fernández- Jiménez A, Pastor JY, Martín A, Palomo A (2010) High- Temperature Resistance in Alkali- Activated Cement. J Am Ceram Soc 93(10):3411-3417. https://doi.org/10.1111/j.1551-2916.2010.03887.x

9. Martin A, Pastor JY, Palomo A, Jiménez AF (2015) Mechanical behaviour at high temperature of alkali activated aluminosilicates (geopolymers). Constr Build Mat er 93:1188-1196. https://doi.org/10.1016/j.conbuildmat.2015.04.044

10. Guerrieri M, Sanjayan JG (2010) Behavior of combined fly ash/slag-based geopolymers when exposed to high temperatures. Fire Mater 34(4):163–175. https://doi.org/10.1002/fam.1014

11. Pan Z, Sanjayan JG, Rangan BV (2009) An investigation of the mechanisms for strength gain or loss of geopolymer mortar after exposure to elevated temperature. J Mater Sci 44 (7):1873-1880. https://doi.org/10.1007/s10853-009-3243-z

12. Rivera OG, Long WR, Weiss Jr CA, Moser RD, Williams BA, Torres-Cancel K, Gore ER, Allison PG (2016) Effect of elevated temperature on alkali-activated geopolymeric binders compared to portland cement-based binders. Cem Concr Res 90:43-51. https://doi.org/10.1016/j.cemconres.2016.09.013

13. Zhao R, Sanjayan JG (2011) Geopolymer and Portland cement concretes in simulated fire. Mag Concr Res 63:163–173. http://dx.doi.org/10.1680/macr.9.00110

14. Rickard WDA, Temuujin J, van Riessen, A (2012) Thermal analysis of geopolymer pastes synthesized from five fly ashes of variable composition. J Non-Cryst solids 358(15):1830-1839. https://doi.org/10.1016/j.jnoncrysol.2012.05.032

15. Li YL, Zhao XL, Raman RS, Al-Saadi S (2018) Thermal and mechanical properties of alkali-activated slag paste, mortar and concrete utilizing seawater and sea sand. Constr Build Mater 159:704-724. https://doi.org/10.1016/j.conbuildmat.2017.10.104

16. Mohabbi Yadollahi M, Dener M (2019) Investigation of elevated temperature on compressive strength and microstructure of alkali activated slag based cements. Eur J Environ Civil Eng:1-15. https://doi.org/10.1080/19648189.2018.1557562

17. Kong DL, Sanjayan JG (2010) Effect of elevated temperatures on geopolymer paste, mortar and concrete. Cem Concr Res 40:334-339. http://dx.doi.org/10.1016/j.cemconres.2009.10.017

18. Kong DLY, Sanjayan JG, Sagoe-Crentsil K (2008) Factors affecting the performance of metakaolin geopolymers exposed to elevated temperatures. J Mater Sci 43(3): 824-831. https://doi.org/10.1007/s10853-007-2205-6

19. Adak D, Sarkar M, Mandal S (2017) Structural performance of nano-silica modified fly ash based geopolymer concrete. Constr Build Mater 135:430-439. https://doi.org/10.1016/j.conbuildmat.2016.12.111.

20. Sarker PK (2011) Bond strength of reinforcing steel embedded in fly ash-based geopolymer concrete. Mater Struct 44(5):1021-1030. https://doi.org/10.1617/s11527-010-9683-8

21. Castel A, Foster SJ (2015) Bond strength between blended slag and Class F fly ash geopolymer concrete with steel reinforcement. Cem Concr Res 72:48-53. https://doi.org/10.1016/j.cemconres.2015.02.016

22. Sofi M, van Deventer JSJ, Mendis PA, Lukey GC (2007) Bond performance of reinforcing bars in inorganic polymer concrete (IPC). J Mater Sci 42(9):3107 3116. https://doi.org/10.1007/s10853-006-0534-5

23. Dewi ES, Ekaputri JJ (2017) The influence of plain bar on bond strength of geopolymer concrete. In: AIP Conference Proceedings, AIP Publishing, 1855(1), 030017. https://doi.org/10.1063/1.4985487

24. Fernandez-Jimenez AM, Palomo A, Lopez-Hombrados C (2006) Engineering properties of alkali-activated fly ash concrete. ACI Mater J 103(2):106-112.

25. Al-Azzawi M, Yu T, Hadi MN, (2018) Factors Affecting the Bond Strength Between the Fly Ash-based Geopolymer Concrete and Steel Reinforcement. Structures 14:262-272. https://doi.org/10.1016/j.istruc.2018.03.010

26. Zhang HY, Kodur V, Wu B, Yan J, Yuan ZS (2018) Effect of temperature on bond characteristics of geopolymer concrete. Constr Build Mater 163:277-285. https://doi.org/10.1016/j.conbuildmat.2017.12.043

27. Ramagiri KK, Kar A (2019) Effect of precursor combination and elevated temperatures on the microstructure of alkali-activated binder. ICJ 93(10):34-43.

28. ASTM C618-19 (2019) Standard Specification for Coal Fly Ash and Raw or Calcined Natural Pozzolan for Use in Concrete. https://doi.org/10.1520/C0618-19

29. ASTM C989 / C989M-18a (2018) Standard Specification for Slag Cement for Use in Concrete and Mortars. https://doi.org/ 10.1520/C0989_C0989M-18A

30. IS 383 (2016) Coarse and Fine Aggregate for Concrete – Specification. .

31. Kar A, Halabe UB, Ray I, Unnikrishnan A (2013) Nondestructive characterizations of alkali activated fly ash and/or slag concrete. Eur Sci J 9(24). http://dx.doi.org/10.19044/esj.2013.v9n24p%25p

32. El-Hassan H, Ismail N (2018) Effect of process parameters on the performance of fly ash/GGBS blended geopolymer composites. J Sust Cem Based Mat 7(2):122-140. https://doi.org/10.1080/21650373.2017.1411296

33. El-Hassan H, Shehab E, Al-Sallamin A (2018) Influence of different curing regimes on the performance and microstructure of alkali-activated slag concrete. J Mater Civ Eng 30(9):04018230. https://doi.org/10.1061/(ASCE)MT.1943-5533.0002436

34. Ismail I, Bernal SA, Provis JL, Hamdan S, van Deventer JS (2013) Microstructural changes in alkali activated fly ash/slag geopolymers with sulfate exposure. Mater Struct 46(3):361-373. https://doi.org/10.1617/s11527-012-9906-2

35. ASTM E119-16 (2016) Standard Test Methods for Fire Tests of Building Construction and Materials. https://doi.org/ 10.1520/E0119-16

36. Park SM, Jang JG, Lee NK, Lee HK (2016) Physicochemical properties of binder gel in alkali-activated fly ash/slag exposed to high temperatures. Cem Concr Res 89: 72-79. https://doi.org/10.1016/j.cemconres.2016.08.004

37. Sarker PK, Kelly S, Yao Z (2014) Effect of fire exposure on cracking, spalling and residual strength of fly ash geopolymer concrete. Mater Des 63: 584-592. https://doi.org/10.1016/j.matdes.2014.06.059

38. ASTM C39/C39M-11 (2011) Standard Test Method for Compressive Strength of Cylindrical Concrete Specimens. https://doi.org/10.1520/C0039_C0039M-11

39. IS 2770-1 (1967) Methods of testing bond in reinforced concrete, Part 1: Pull-out test.

40. Kumar S, Kumar R, Mehrotra SP (2010) Influence of granulated blast furnace slag on the reaction, structure and properties of fly ash based geopolymer. J Mater Sci 45(3):607-615. https://doi.org/10.1007/s10853-009-3934-5

41. Fang G, Ho WK, Tu W, Zhang M (2018) Workability and mechanical properties of alkali-activated fly ash-slag concrete cured at ambient temperature. Constr Build Mater 172:476-487. https://doi.org/10.1016/j.conbuildmat.2018.04.008

42. Shaikh FUA (2018) Effects of slag content on the residual mechanical properties of ambient air-cured geopolymers exposed to elevated temperatures. J Asian Ceram Soc 6(4):342-358. https://doi.org/10.1080/21870764.2018.1529013

43. Junaid MT, Kayali O, Khennane A (2017) Response of alkali activated low calcium fly-ash based geopolymer concrete under compressive load at elevated temperatures. Mater Struct 50(1):50. https://doi.org/10.1617/s11527-016-0877-6

44. Kalifa P, Menneteau FD, Quenard D (2000) Spalling and pore pressure in HPC at high temperatures. Cem Concr Res 30(12):1915-1927. https://doi.org/10.1016/S0008-8846(00)00384-7

45. Provis JL, van Deventer JSJ (eds) (2009) Geopolymers: structures, processing, properties and industrial applications. CRC Press, Cambridge, UK.

46. Zuda L, Pavlík Z, Rovnaníková P, Bayer P, Černý R, (2006) Properties of alkali activated aluminosilicate material after thermal load. Int J Thermophys 27(4):1250-1263. https://doi.org/10.1007/s10765-006-0077-7

47. Kong DL, Sanjayan JG, Sagoe-Crentsil K (2007) Comparative performance of geopolymers made with metakaolin and fly ash after exposure to elevated temperatures. Cem Concr Res 37(12):1583-1589. https://doi.org/10.1016/j.cemconres.2007.08.021

48. Fang G, Zhang M (2020) The evolution of interfacial transition zone in alkali-activated fly ash-
slag concrete. Cem Concr Res 129:105963. https://doi.org/10.1016/j.cemconres.2019.105963

49. Hertz K (1982) The anchorage capacity of reinforcing bars at normal and high temperatures. Mag Concr Res 34(121):213-
220. https://doi.org/10.1680/macr.1982.34.121.213

50. Pothisiri T, Panedpojaman P (2012) Modeling of bonding between steel rebar and concrete at elevated temperatures. Constr Build Mater 27(1): 130-140. https://doi.org/10.1016/j.conbuildmat.2011.08.014

51. Willam K, Xi Y, Lee K, Kim B (2009) Thermal response of reinforced concrete structures in nuclear power plants. A report submitted at College of Engineering and Applied Science, University of Colorado at Boulder.

Figure 1

Click here to access/download;Figure;Fig 1.eps

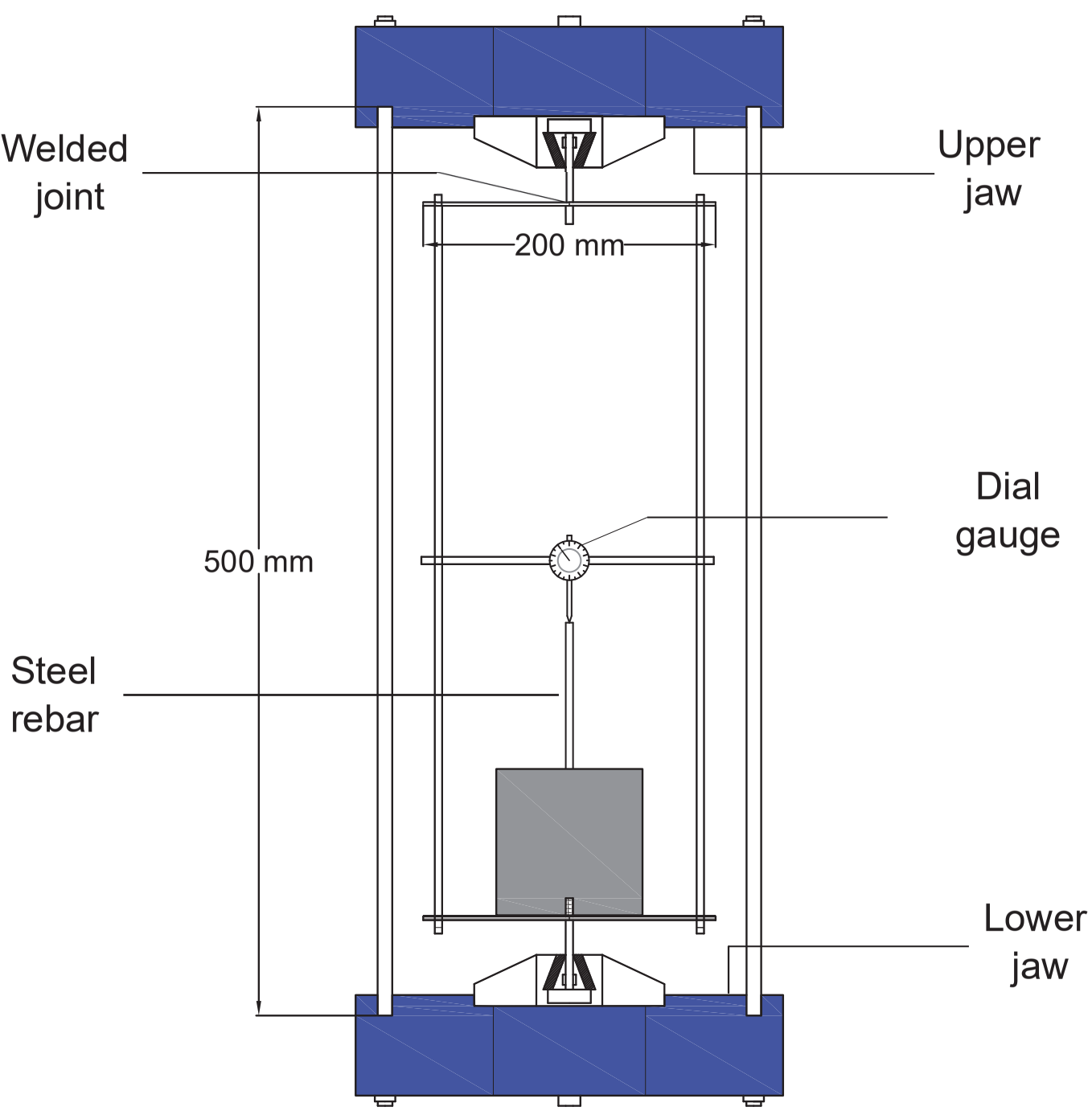

Figure 2

Click here to access/download;Figure;Fig 2.eps

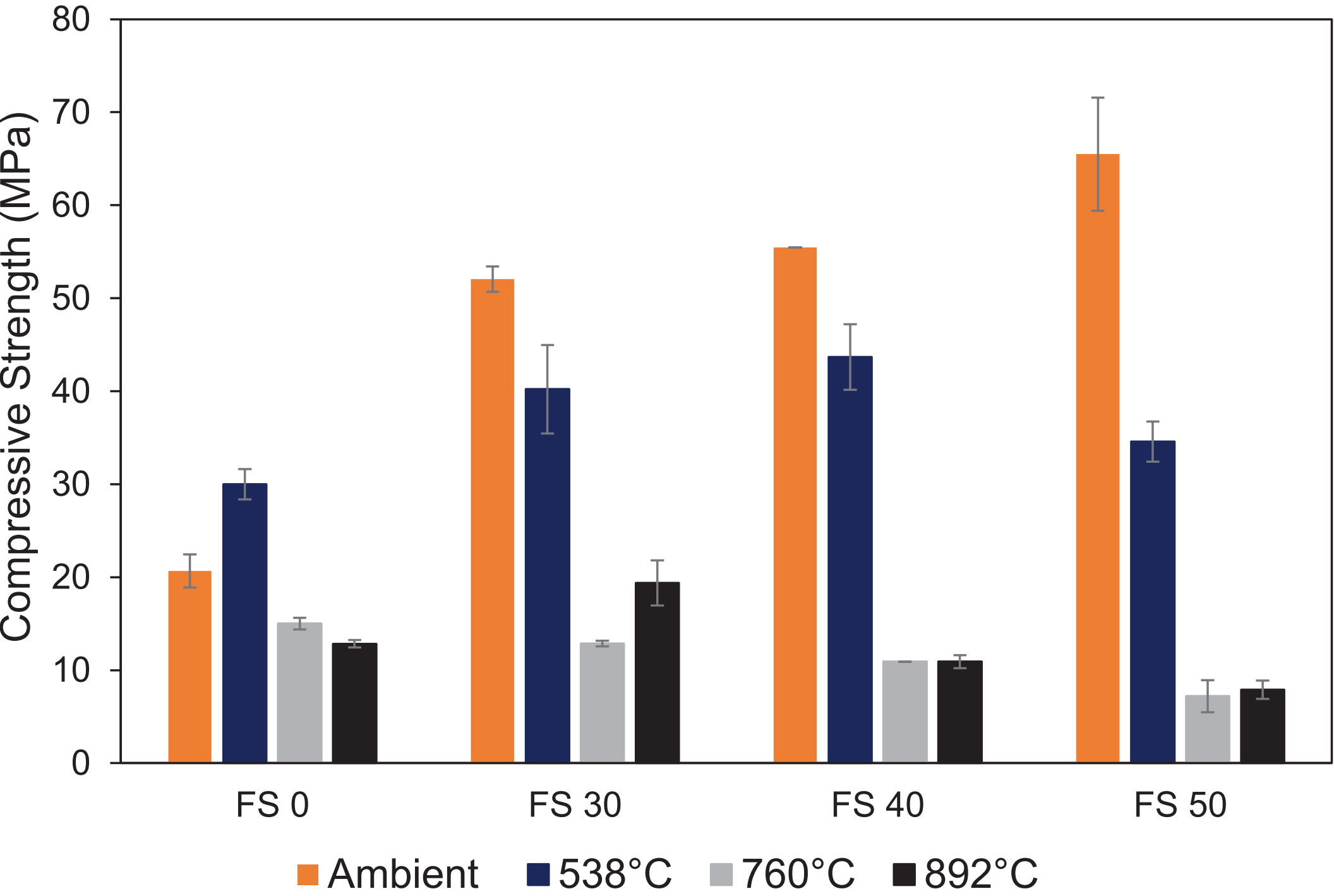

Figure 3a

Click here to access/download;Figure;Fig 3a.eps

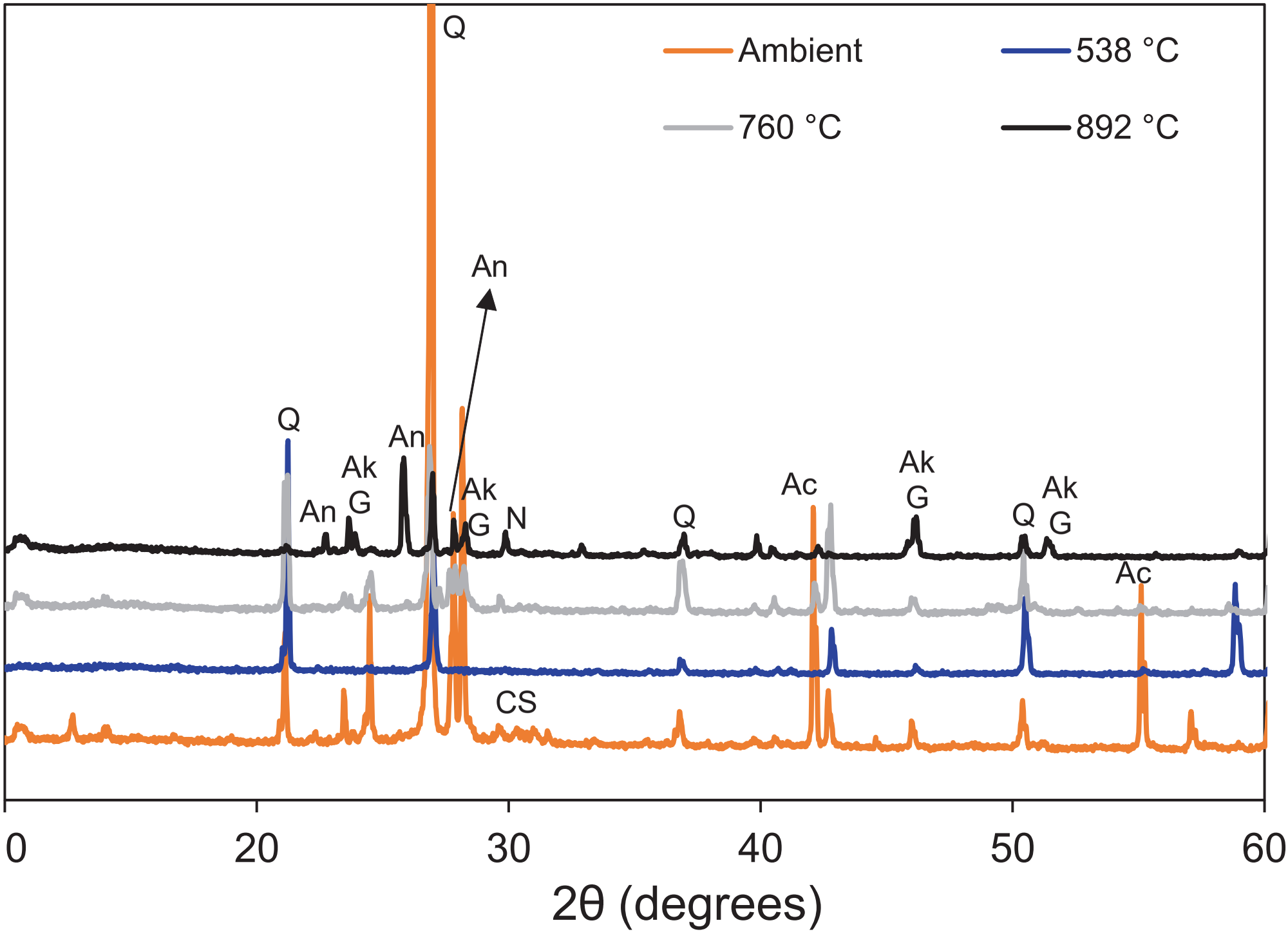

Figure 3b

Click here to access/download;Figure;Fig 3b.eps

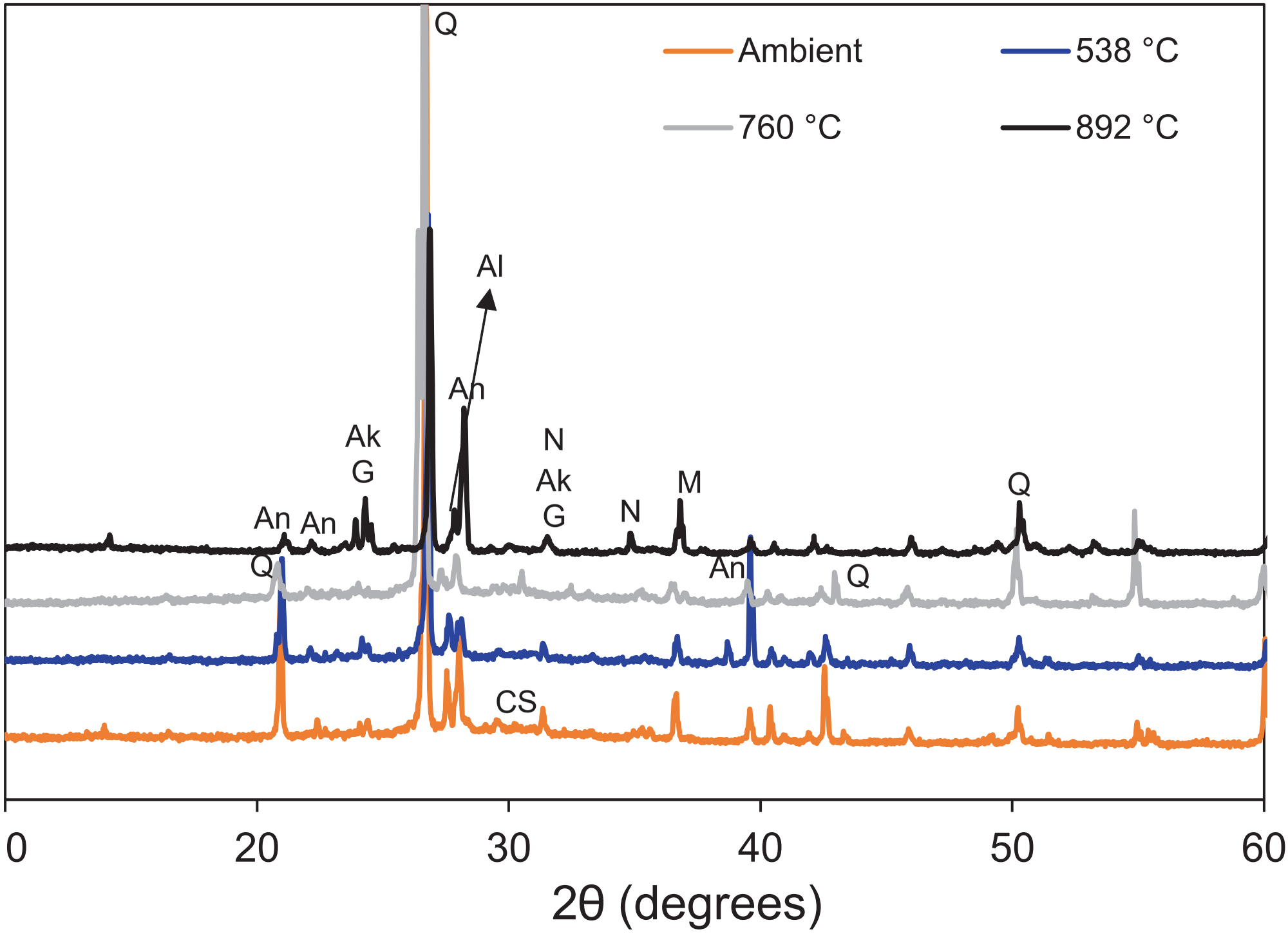

Figure 3c

Click here to access/download;Figure;Fig 3c.eps

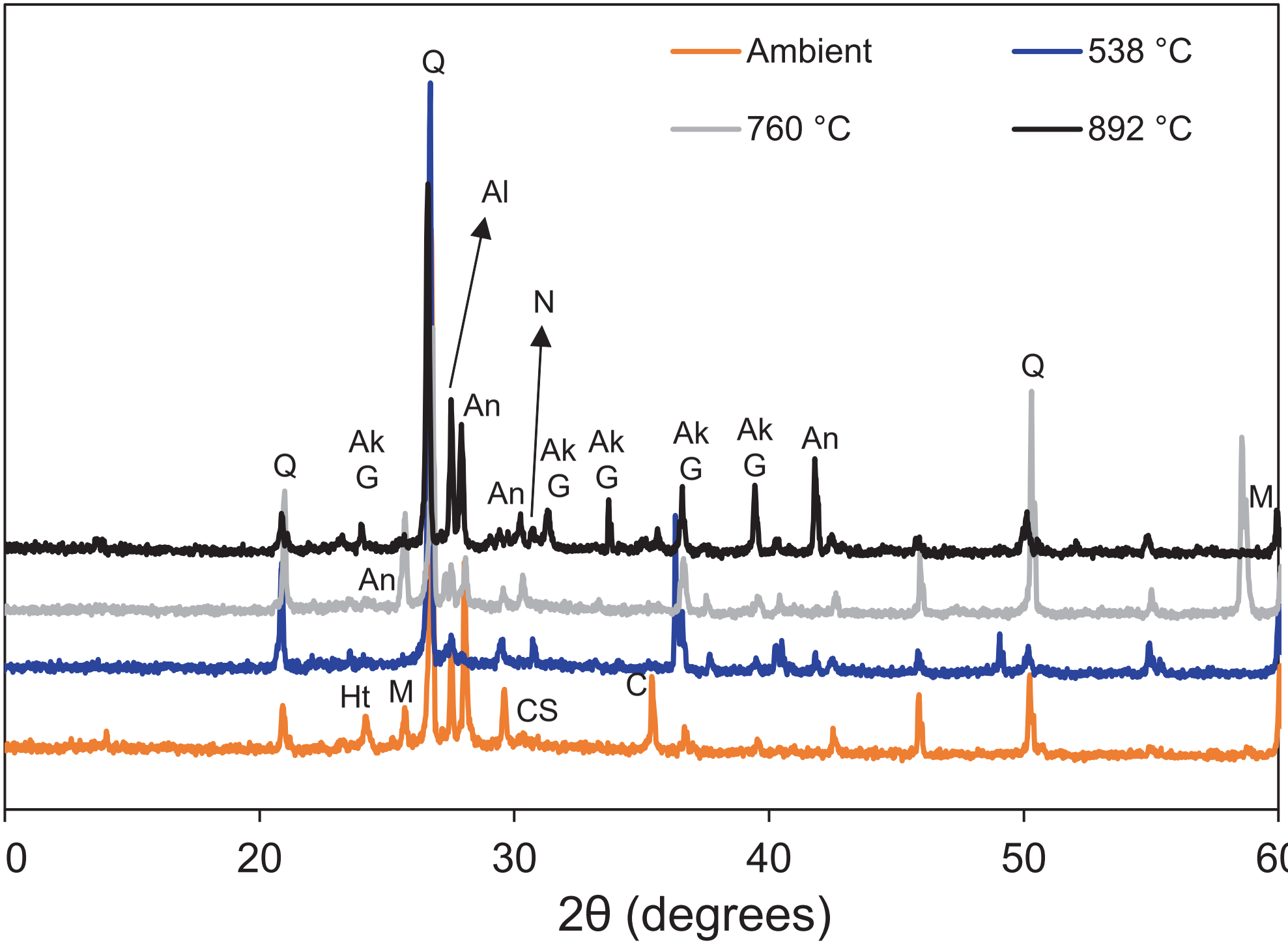

Figure 4

Click here to access/download;Figure;Fig 4.eps

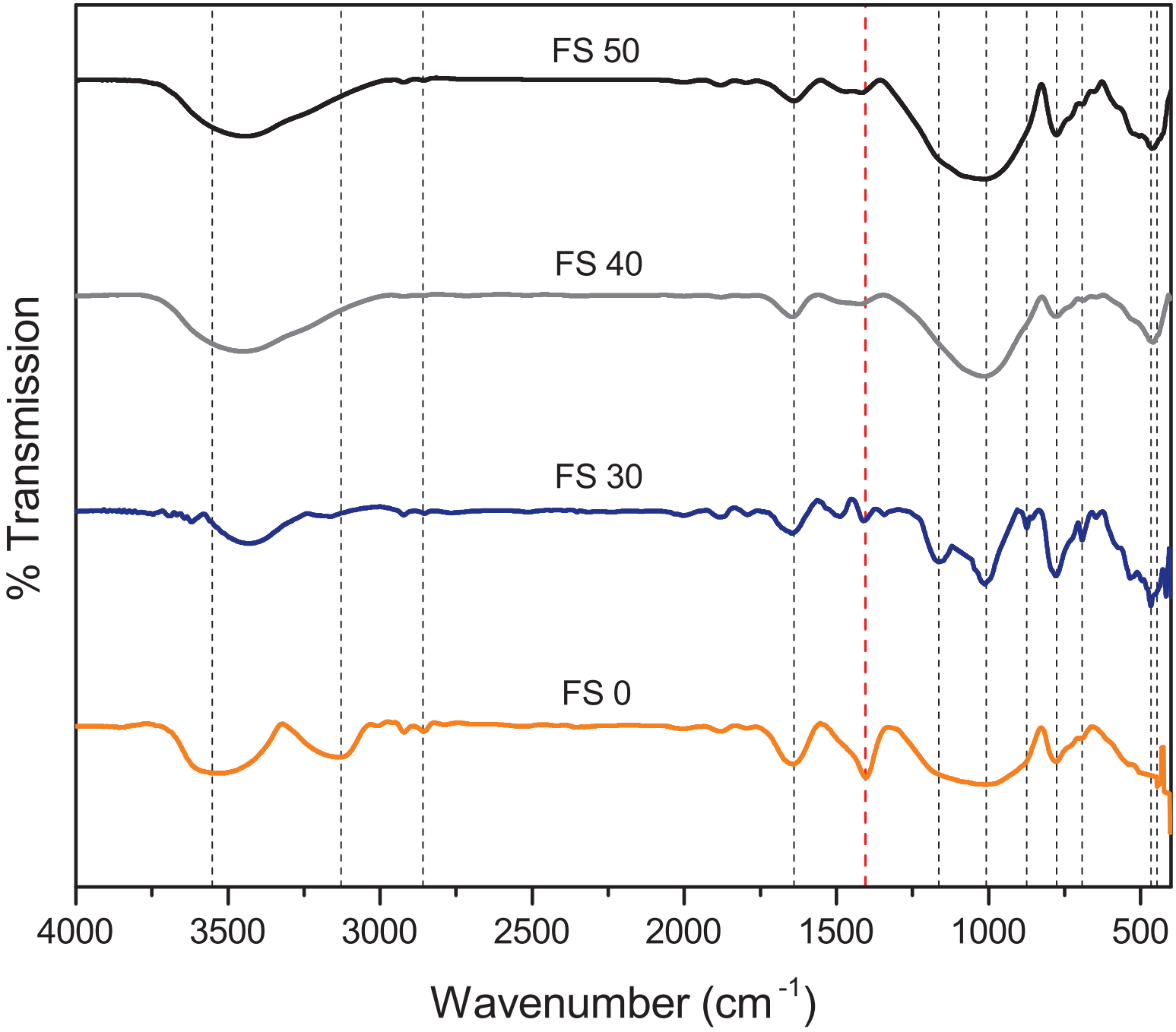

Figure 5

Click here to access/download;Figure;Fig 5.eps

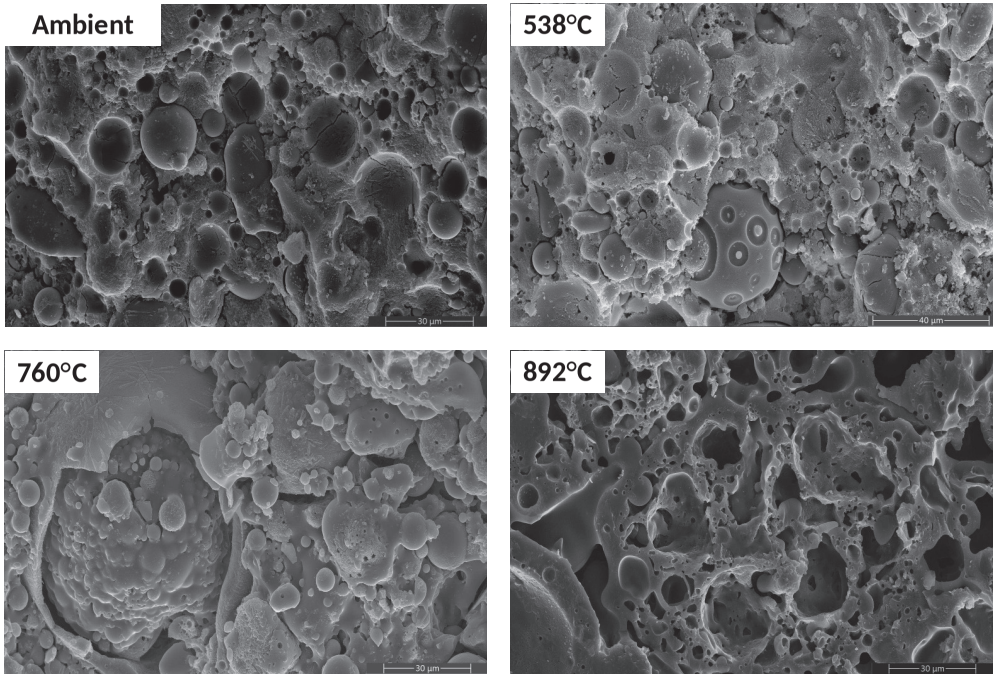

(a) FS 0

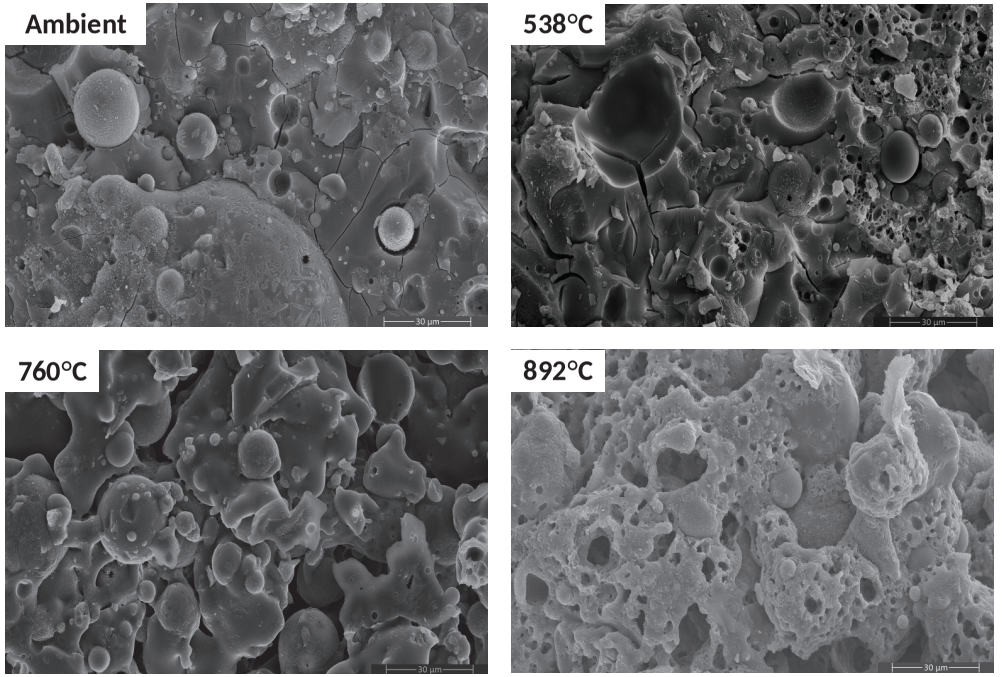

(b) FS 30

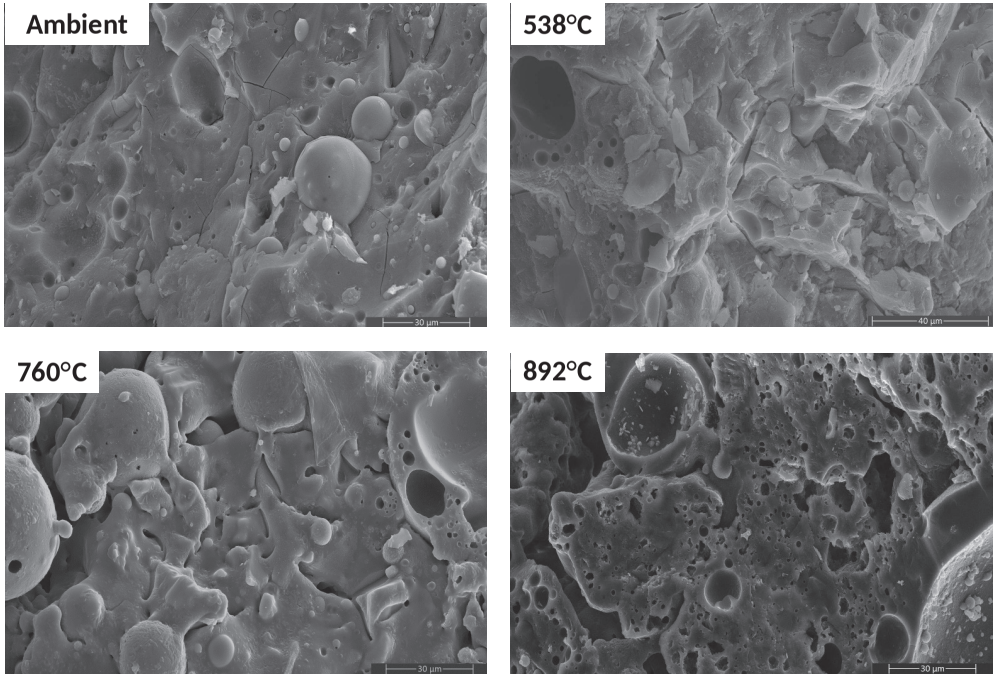

(c) FS 40

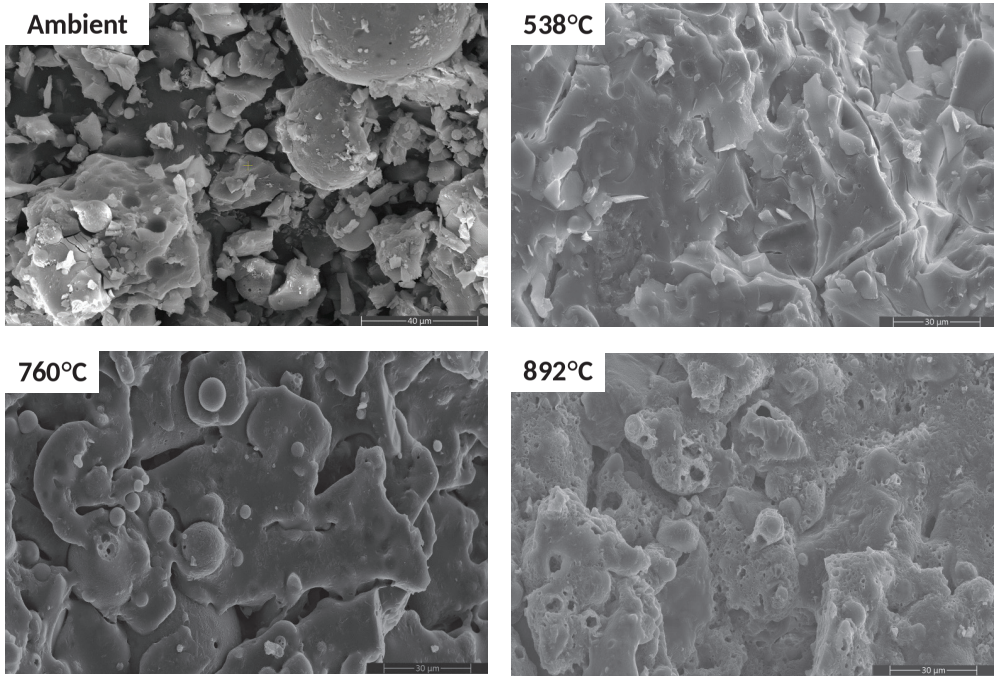

(d) FS 50

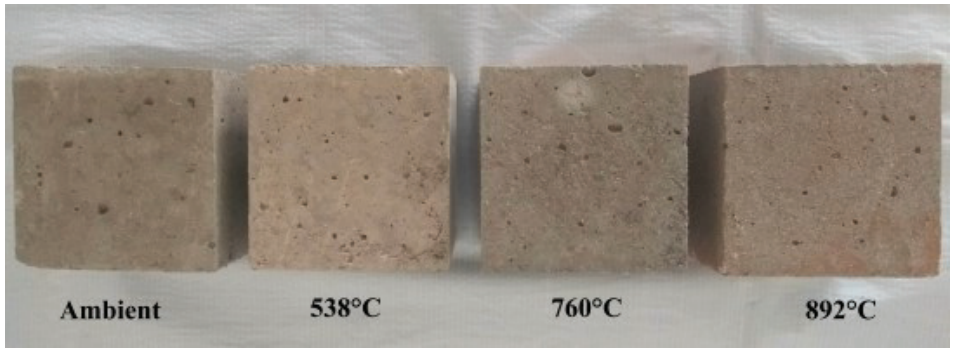

(a) FS 0

(d) FS 0 AT*

(e) FS 0 892°C

(f) FS 30 AT*

(g) FS 30 892°C

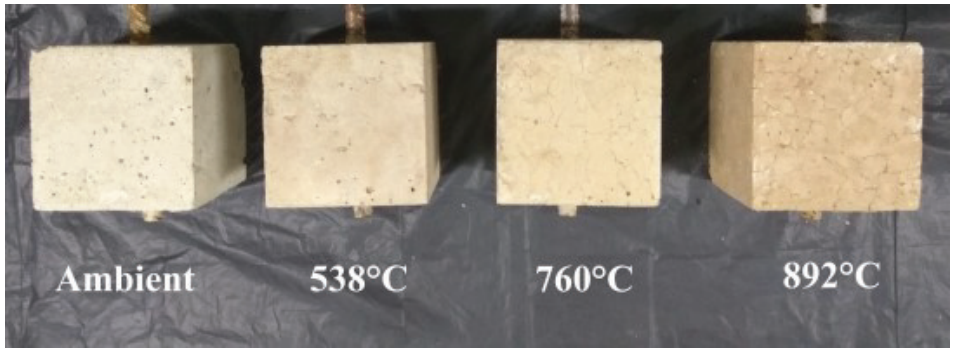

(b) FS 30

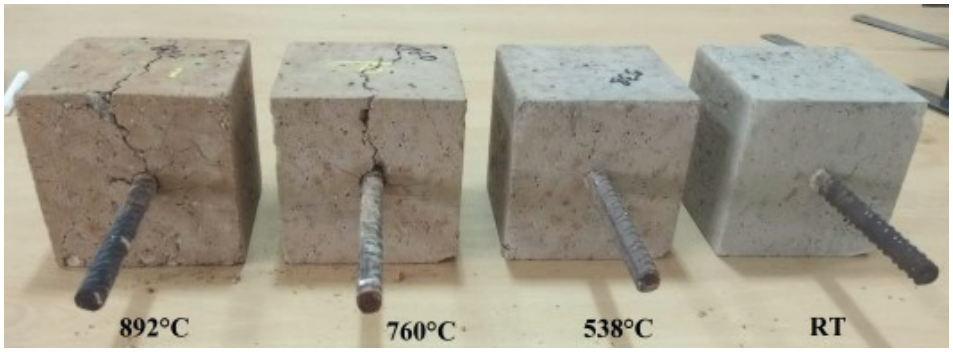

(h) FS 40

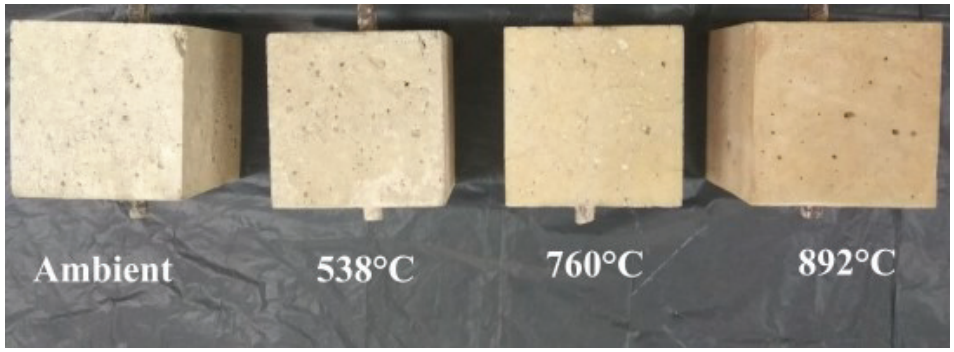

(c) FS 50

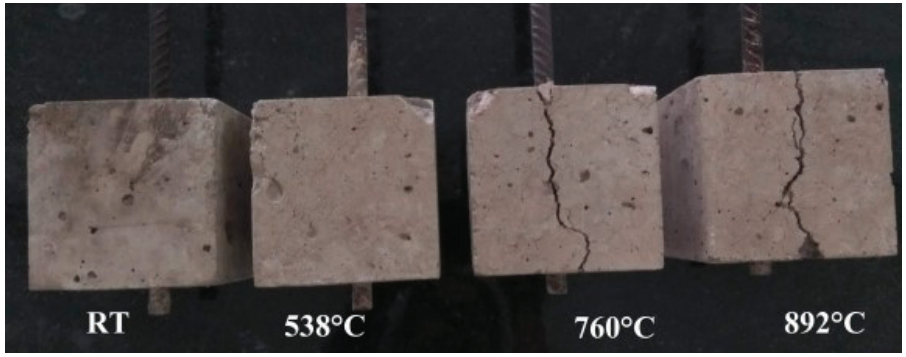

(i) FS 50

Figure 7

Click here to access/download;Figure;Fig 7.eps